HHS Public Access

Author manuscript

ACS Appl Mater Interfaces. Author manuscript; available in PMC 2019 August 22.

Published in final edited form as:

ACS Appl Mater Interfaces. 2018 August 22; 10(33): 27965–27971. doi:10.1021/acsami.8b08868.

TiO_2-Capped Gold Nanorods for Plasmon-Enhanced Production of Reactive Oxygen Species and Photothermal Delivery of Chemotherapeutic Agents

Liangcan He[†], **Chenchen Mao**[‡], **Michael Brasino**[†], **Albert Harguindey**[†], **Wounjhang Park**[‡,§], **Andrew P. Goodwin**[†,§], **Jennifer N. Cha**[*,†,§]

[†]Department of Chemical and Biological Engineering, University of Colorado Boulder, Boulder, Colorado 80303, United States

[‡]Department of Electrical, Computer and Energy Engineering, University of Colorado Boulder, Boulder, Colorado 80303, United States

[§]Materials Science and Engineering Program, University of Colorado Boulder, Boulder, Colorado 80303, United States

Abstract

Near infrared (NIR)-absorbing noble metal nanostructures are being extensively studied as theranostic agents, in particular for photoacoustic imaging and photothermal therapy. Because of the electric field enhancement at the tips of anisotropic metal nanostructures, positioning photoactive species at these sites can lead to increased energy absorption. Herein, we show the site-specific placement of NIR-active photosensitizers at the ends of gold nanorods (AuNRs) by growing porous TiO_2 caps. The surface plasmon resonance of the AuNRs was carefully tuned to overlap with the exciton absorption of indocyanine green (ICG), a NIR photosensitizer with low quantum yields and poor photostability. In conjugating high amounts of ICG to the TiO_2 caps, increased amounts of singlet oxygen ($^1O_2$) were generated as compared to when ICG was attached to sidewalls of the AuNRs. Because the AuNRs also cause local increases in temperature upon NIR excitation, DNA strands were next attached to the AuNRs sidewalls and loaded with doxorubicin (DOX). We found that the synergistic effect of increased $^1O_2$ and photothermal-induced drug delivery led to significant improvements in tumor cell killing. This work demonstrates that with careful design over hybrid nanostructure synthesis, higher levels of tumor therapy may be achieved.

Graphical Abstract

[*]**Corresponding Author** Jennifer.Cha@colorado.edu.

Author Contributions

The manuscript was written through contributions of all authors. All authors have given approval to the final version of the manuscript.

ASSOCIATED CONTENT

Supporting Information

The Supporting Information is available free of charge on the ACS Publications website at DOI: 10.1021/acsami.8b08868.

TEM images; optical photos; UV–vis absorbance spectra; DOX standard concentration–absorption curve; DOX standard concentration–fluorescence curve; and in vitro cell viability (PDF)

The authors declare no competing financial interest.

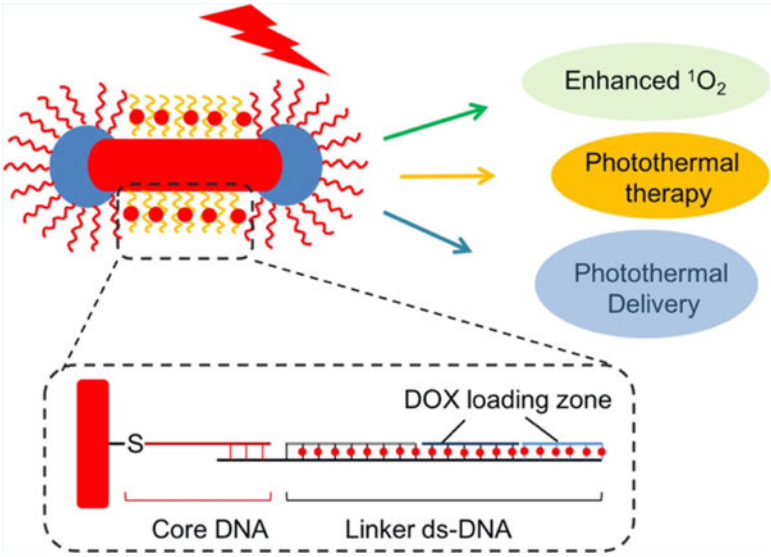

Keywords

TiO_2 capped gold nanorods; plasmon-enhanced; singlet oxygen; photodynamic therapy; photothermal delivery

INTRODUCTION

With rapid developments in nanoscience and nanotechnology, there has been an increased focus on agents that can target, detect, and treat diseased locations in vivo. Photodynamic therapy (PDT) has been widely used because of its minimal invasiveness and ability to confine therapy to a focused area of the patient.[1–9] PDT typically utilizes light-absorbing photosensitizers that under irradiation convert dissolved oxygen into the highly cytotoxic singlet oxygen ($^1O_2$) to elicit cell death through apoptosis and/or necrosis, tumor vasculature damage, and acute inflammatory reactions leading to progressive disease regression.[10–12] For biomedical applications, near-infrared (NIR) light is desired because of its increased tissue penetration depth as compared to UV or visible light. In particular, photosensitizers such as the FDA-approved indocyanine green (ICG) are of interest because of their maximum absorption peak at 808 nm.[2,8] However, ICG is a cyanine dye and as such it suffers from low quantum yield, undesired aggregation, poor photostability, low thermal stability in aqueous solution, and rapid blood clearance.[2,8] In addition, the NIR-triggered photosensitizers usually demonstrate low solubility in saline environments. As a result, high laser fluences are required, which is problematic in deep tissue.

The near-field enhancement of electromagnetic fields created at the vicinity of noble metal nanostructures upon photon irradiation has been used to increase the energy absorbed by optically active molecules and materials.[13] In particular, gold nanomaterials have been widely explored in the field of chemical sensing,[13–15] catalysis,[16–19] and nanomedicine.[12,20,21] The enhanced electric fields have, for example, been used to increase upconversion efficiencies in upconverting nanoparticles by placing them site-specifically at the tips of Au

nanostars.[22] Although a similar phenomenon should be observed using NIR-absorbing photosensitizers, controlling the placement of such molecules site-specifically on a gold nanostructure has been difficult to achieve.[2,23,24] To mitigate this, we show here the synthesis and use of gold nanorods (AuNRs) that show strong plasmon resonances at NIR wavelengths and with mesoporous TiO_2 caps at the ends of the NRs. The NIR-absorbing photosensitizer ICG was selectively conjugated to the TiO_2 caps using copper-free click chemistry (Figure 1). Enhanced $^1O_2$ was produced upon 808 nm photoirradiation when the ICG groups were placed at the ends of the AuNRs through the TiO_2 caps (AuNR@TiO_2-ICG) as compared to when the ICG molecules were attached to the AuNR sidewalls (ICG-AuNR@TiO_2). The amount of $^1O_2$ produced is known to be dependent on the distance between the photosensitizer used and the Au surface.[13,23] At very short distances, Au will quench the $^1O_2$ emission; at intermediate distances, an enhancement of the $^1O_2$ produced can be observed because of the effect of the surface plasmon but this enhancement factor falls off with increasing distance finally leveling off.[23] Next, as an additional therapy modality, the TiO_2-capped AuNRs were further studied as a photothermal agent for releasing anticancer drugs by conjugating double-stranded DNA (dsDNA) to the long sides of the AuNRs and loading the anticancer agent doxorubicin (DOX) (Figure 1).[25] The increase in $^1O_2$ production by placing ICG specifically at the tips of the AuNRs coupled with the photothermal-induced DOX release yielded an enhanced therapeutic effect on MDA-MB-468 cancer cells because of the combined photodynamic, photothermal, and chemotherapy effect. These studies show that hybrid gold–metal oxide nanostructures can be used to control the spatial distribution of individual therapy agents for enhanced multimodal therapy.

EXPERIMENTAL SECTION

Materials.

All materials and solvents were used as received without further purification. Dulbecco's modified Eagle's medium (DMEM) (high glucose with $_L$-glutamine sterile-filtered) and fetal bovine serum (FBS) were purchased from Sigma-Aldrich. Hexadecyltrimethylammonium bromide (CTAB), $_L$-ascorbic acid (AA) (99.9%), silver nitrate (99%), gold(III) chloride trihydrate (99.9%), sodium oleate (NaOL, >95%), $TiCl_3$ (12%), poly(ethylene glycol) (PEG)-SH (2000), 2,3-bis(2-methoxy-4-nitro-5-sulfophenyl)-2*H*-tetrazolium-5-carboxanilide (XTT), phenazine methosulfate (PMS), *N*-hydroxysuccinimidyl–dibenzocyclooctyne (NHS–DBCO), dopamine, and 9,10-anthracenediyl-bis(methylene) dimalonic acid (ABDA) were purchased from Sigma-Aldrich. Sodium bicarbonate ($NaHCO_3$, 99%), sodium borohydride ($NaBH_4$, 99%), and hydrochloric acid (HCl) (36.5–38% in water) were purchased from Fisher Scientific. The azide-ICG was bought from Intrace-medical. All of the chemicals were used as received without further purification. The DNA was purchased from Integrated DNA Technologies Inc. DOX hydrochloride was bought from Tokyo Chemical Industry Co. Ltd. NHS–mPEG was bought from Laysan Bio, Inc. Deionized water was used throughout the experiments.

Synthesis of AuNRs.

In this work, the AuNRs were synthesized using methods described by Murray et al. with some minor modifications.[26]

1. Au seed solution: 5 mL of 0.2 M CTAB solution was mixed with 5 mL of 0.5 mM $HAuCl_4$ in a 20 mL scintillation tube. Afterward, 0.6 mL of freshly prepared 0.1 M $NaBH_4$ solution (ice-cooled) was injected rapidly into the solution mixture. The solution was stirred for 2 min and left to stand at 30 °C for 30 min before use.
2. Growth solution: the stock solution of surfactants was prepared by dissolving 3.6 g of CTAB and 0.4936 g of NaOL into 100 mL of water at 90 °C with vigorous stirring. The solution was then cooled to room temperature before use. In a typical AuNR synthesis, the surfactant solution was mixed with 9.6 mL of 4 mM $AgNO_3$ solution and kept undisturbed at 30 °C for 15 min. Then, 100 mL of 1 mM of $HAuCl_4$ solution was added and stirred for 90 min followed by adding 1.2 mL of HCl (37 wt %) and stirring for 15 min. After that 0.5 mL of 0.064 M AA solution was injected and 50 μL of the Au seed solution was added; the mixture solution was then maintained at 30 °C for 12 h. The final products were isolated by centrifugation at 6000 rpm for 30 min followed by removal of the supernatant.

Synthesis of TiO_2-Capped AuNR Nanostructures.[27]

In a typical synthesis, 10 μL of 12% $TiCl_3$ was diluted with 150 μL of degased H_2O in a 10 mL centrifuge tube. Then, 45 μL of 1 M $NaHCO_3$ was added to the solution dropwise under stirring. Before the addition of last two or three drops of bicarbonate, the solution turns into a dark blue solution. The pH of this solution was around 2.6. Afterward, a mixture of 120 μL of AuNR stock solution (7.6 nM), 18 μL of 0.2 M CTAB solution, and 17 μL of water was added into the above dark blue solution. The dispersion was then gently stirred/shaked for 20 min. The product was collected by centrifuging at 6000 rpm for 10 min and washed with ethanol twice.

ICG Conjugation To AuNR@TiO_2.

The prepared AuNR@TiO_2 was first reacted with dopamine at the ratio of 1:20 000 = AuNR/dopamine. After 3–5 hours of reaction, the amine-modified AuNRs were purified by centrifugation and redispersed in water solution. Then, the amine-AuNRs were reacted with an excess of NHS–DBCO at a ratio of 1:30 000 (AuNR/NHS–DBCO) for 5 h, followed by centrifugation. After that the AuNRs@TiO_2 (DBCO modified) samples were reacted with azide-ICG at the ratio of 1:12 000 (AuNR/ICG) overnight. The conjugated ICG per AuNR was determined by the standard curve of ICG (absorption–concentration curve). At last, 10 mg of NHS–PEG (20 000) was reacted with AuNR@TiO_2-ICG overnight and then the products were purified for further use.

For conjugating ICG to the AuNR sidewalls (ICG-AuNR@TiO_2), the AuNR@TiO_2 nanoparticles were first reacted with dopamine (1:20 000 = AuNR/dopamine). After a few hours, the samples were mixed with NHS–DBCO followed by reacting with 10 mg of NHS–

PEG overnight. Next, the PEG-conjugated AuNR@TiO_2 was reacted overnight with cysteamine using a 30 000:1 cysteamine/nanoparticle molar ratio followed by reacting with NHS–DBCO for 3–5 h. The products were then purified by centrifugation and next reacted with azide-ICG using a 1:10 000 AuNR@TiO_2/ICG molar ratio for 12 h. The amount of ICG attached per AuNR was determined using a standard absorption curve of ICG.

Singlet Oxygen Generation Test.

The dye ABDA was employed for measuring the production of singlet oxygen upon 380 nm excitation. Once singlet oxygen generates, the ABDA fluorescence would become quenched, and this decay could be measured and plotted as a function of irradiation time to the NIR laser. The concentrations of ICG in either the mix of ICG and AuNR@TiO_2, ICG-AuNR@TiO_2, or AuNR@TiO_2-ICG were kept equivalent. Before 808 nm laser irradiation, 2.4 μL of 2 mM ABDA dimethyl sulfoxide (DMSO) solution (ICG/ABDA = 1:1) was added. Then, the samples were irradiated with 808 nm light (60 mW cm^{-2}) for 0, 5, 10, 15, and 25 min. At every time point, 100 μL of the solution was taken out and centrifuged. The fluorescence intensity of the supernatant was obtained on a fluorimeter using 380 nm excitation and reading emission at 430 nm. All of the samples were prepared in triplicate.

DNA Functionalization of AuNR@TiO_2-ICG.

The purified AuNR@TiO_2-ICG was mixed with tris(2-carboxyethyl)phosphine-reduced thiol-DNA (HS-AAA AAA AAA ACC TAT CGA CCA TGC T) at a ratio of 1:2000 (AuNR@TiO_2/thiol-DNA = 1:2000) and sodium dodecyl sulfate (0.2%). The mixture was incubated for 20 min; then, TBE buffer (2×, pH = 3.0, 1 M NaCl) was added. The resulting solution was reacted overnight and then purified by centrifugation.

DNA Hybridization on the Sidewall of AuNR@TiO_2-ICG.

The 1200 μL 2.1 nM thiol-DNA-modified AuNR@TiO_2-ICG sample was mixed with 20 μL of 200 μM linker single-stranded DNA (ssDNA) (GAG GGA TCG TTG TTA TTC GTG TTC GTA TTC GTA TTC GTT CGT TAG CAT GGT CGA TAG G) in phosphate-buffered saline (PBS) buffer (10×, $MgCl_2$ 50 mM, 0.01% TWEEN 20). The solution was heated at 60 °C for 10 min, followed by cooling down at the rate of 1 °C/min to 37 °C and maintained at this temperature for 1 h, and then cool down to 4 °C. The linker ssDNA-functionalized AuNR@TiO_2-ICG was washed with PBS buffer three times and redispersed in PBS buffer (10×, $MgCl_2$ 50 mM, 0.01% TWEEN 20). The purified linker ssDNA-modified AuNR@TiO_2-ICG was then hybridized with 20 μL of 200 μM DOX middle zone complementary DNA strands (DNA1, DNA2, and DNA3) in sequence in PBS buffer (10×, $MgCl_2$ 50 mM, 0.01% TWEEN 20) at 37 °C for 1 h and then cool down to 4 °C. Finally, the DNA-hybridized AuNR@TiO_2-ICG was purified by centrifugation and washed with PBS buffer three times. At last, the samples were redispersed in PBS buffer and maintained at 4 °C for further use.

Thiol-DNA: 5′-thiol-AAA AAA AAA ACC TAT CGA CCA TGC T-3′

Linker ssDNA: 5′-GAG GGA TCG TTG TTA TTC GTG TTC GTA TTC GTA TTC GTT CGT TAG CAT GGT CGA TAG G-3′

DNA1: 5′-ACG AAC GAA TAC G-3′

DNA2: 5′-AAT ACG AAC ACG AA-3′

DNA3: 5′-TAA CAA CGA TCC CTC-3′

DOX Loading and Quantification in DNA-Functionalized AuNR@TiO_2-ICG.

Stock solution (80 μL) of DNA-functionalized AuNR@TiO_2-ICG (containing 32.0 nM AuNRs) was mixed with 80 μL of DOX DMSO solution at the ratio of 1:10 000 (AuNR/DOX). The mixture was incubated at room temperature for 8 h. The DOX-loaded AuNR@TiO_2-ICG was purified via centrifugation and washing in PBS buffer three times.

To calculate the amount of loaded DOX per AuNR@TiO_2-ICG nanostructure, the relevant standard concentration curve was prepared and correlated with the DOX absorption peak around 480 nm. For this, the stock PBS solution of DOX-AuNR@TiO_2-ICG nanocomposites was heated to 65 °C for 30 min and released DOX was collected and the concentration was calculated by measuring the absorption spectra and correlated with the standard concentration–absorption curve. It was found that there were ~2278 ± 528 DOX molecules loaded in per AuNR@TiO_2-ICG nanostructure. All of the samples were prepared in triplicate.

DOX Release Test.

DOX-loaded AuNR@TiO_2-ICG nanostructures (8.5 nM AuNR) were prepared and purified by centrifugation for multiple times. The solution was maintained at 37, 47 °C, or irradiated with 808 nm laser light, and the supernatant was collected at different time points (0, 5, 10, 15, 20, and 25 min) and quantified for the amount of the released DOX by measuring the fluorescence peak around 590 nm (excitation at 480 nm). All of the samples were prepared in triplicate.

Cell Culture.

The MDA-MB-468 cells were grown to confluence at 37 °C and with 5% CO_2 in DMEM containing 10% FBS and 1% penicillin/streptomycin.

Cytotoxicity Assay (XTT Assay).

The MDA-MB-468 cells were cultured in a 96-well microplate with DMEM containing 10% FBS and 1% penicillin/streptomycin with a density of 1×10^4 cells/well. They were maintained at 37 °C in a humidified atmosphere of 95% air and 5% CO_2. After 12 h, serial dilutions of ICG and AuNR@TiO_2, their mixture, and ICG-conjugated samples (with and without DOX loading) were, respectively, added to the culture wells with a final volume of 100 μL to replace the original culture medium (equivalent ICG concentration is 7.5 μM). After continuous exposure to the nanomaterials for 5 h, the cell viability was determined using a XTT assay. The culture medium was removed and replaced by 100 μL of fresh culture medium followed by adding 25 μL of XTT/PMS solution: 4 mg of XTT + 4 mL of medium + 10 μL of 10 mM PMS). The cells were then incubated for 4 h at 37 °C in the CO_2

incubator. The quantification of cell viability was performed using the optical absorbance (450/650 nm) with the microplate reader. All of the samples were prepared in triplicate.

Toxicity Measurement of DOX-AuNR@TiO_2-ICG.

A 96-well plate was incubated with 1×10^4 cells/well in triplicates and kept in an incubator overnight. The old medium was removed and DOX and AuNR@TiO_2-ICG with and without DOX-loading samples in DMEM were incubated for 5 h (equivalent DOX concentrations of 0.5, 1.0, 2.0, 5.0, and 10.0 μM). The solution was removed and followed by cell washing; then, XTT assay was carried out as mentioned above. All of the samples were prepared in triplicate.

Photodynamic and Photothermal Test.

MDA-MB-468 cells were incubated with ICG, DOX, AuNR@TiO_2, and AuNR@TiO_2-ICG conjugation with and without DOX loading and mixture samples at a final AuNR@TiO_2 concentration of 1.2 nM for 5 h; excess samples were removed by PBS washing and 100 μL of fresh medium was added. Then, an 808 nm laser (808 nm laser spot size: 2 mm in diameter. Laser power: 100 mW, and laser confluence: 3.18 W cm^{-2}) was used to irradiate each cell well in the 96-well plate for 15 min and then replaced with fresh culture medium and cultivated for another 12 h at 37 °C to determine the effects of the 808 nm light irradiation and light-induced $^1O_2$ on cell viability. Cell viability was determined by XTT assay. All of the samples were prepared in triplicate.

RESULTS AND DISCUSSION

In this study, we first report a wet-chemistry method for the anisotropic growth of TiO_2 at the tips of AuNRs and their use to place the NIR photosensitizer ICG at sites where the local field enhancement is greatest upon 808 nm photoirradiation.[27] For this, AuNRs were first synthesized using methods developed by Murray et al. with minor modifications.[26] As shown in Figure 2, the AuNRs had an average length of 91.2 ± 7.3 nm with widths of 26.7 ± 2.0 nm, corresponding to a mean aspect ratio of ~3.4 giving a longitudinal surface plasmon resonance (SPR) maximum ~800 nm, which has a strong resonance overlap with the ICG photosensitizer. Next, the TiO_2 caps were nucleated and grown at the AuNR tips using procedures published by Stucky and co-workers.[27]

After carefully optimizing the $TiCl_3$ hydrolysis rate by using a final pH of 2.6, we were able to obtain AuNRs that possessed TiO_2 caps at the tips with ~21 nm thickness (Figure 2b). Utilizing lower or higher pH values led to either incomplete formation of TiO_2 caps or too thick of a layer of TiO_2 (Figure S1). Although the longitudinal SPR maximum showed a red shift to ~825 nm after the TiO_2 synthesis, a strong resonance overlap with ICG still remained.

To conjugate the ICG photosensitizer specifically to the TiO_2 caps on the AuNRs, dopamine was used, which is known to form two O–Ti bonds with two surface Ti sites.[28] After reacting dopamine with the TiO_2-capped AuNRs (AuNR@ TiO_2) for 3–5 h, the solution color and UV–vis spectra changed (Figures S2, S3 and 2), confirming the conjugation of dopamine with the TiO_2 surface. The dopamine-modified AuNR@TiO_2 was next reacted

with NHS–DBCO at room temperature for 5 h. To attach the ICG to the TiO_2 caps, azide-functionalized ICG (Intrace Medical SA, Switzerland) was reacted overnight with the DBCO-modified AuNR@TiO_2 in DMSO–water (1:1) mixture solution using 1:12 000 AuNR@TiO_2/ICG molar ratios. The products were then purified using multiple microcentrifuge filtrations and UV–vis was used to determine that ~6583 ± 567 ICG molecules were attached to each AuNR@TiO_2 (AuNR@TiO_2-ICG) (Figure S4). The ICG-modified nanoparticles were next reacted with excess of PEG–NHS (MW 20 000) to block any free amine groups remaining on the TiO_2 caps as well as to improve biocompatibility. As shown in Figure 2c, after conjugating ICG to the ends of AuNRs@TiO_2, the localized SPR peak of AuNR@TiO_2-ICG slightly red-shifted. In contrast, a simple mixture of AuNR@TiO_2 and ICG showed no such shift in absorption of the AuNRs (Figure S3), indicating that the direct conjugation of ICG to the TiO_2 caps was successful and affected the overall SPR.

Next, the AuNR@TiO_2-ICG nanostructures were tested for $^1O_2$ production. To determine the effect of attaching ICG site-specifically to the AuNR tips and its effect on $^1O_2$ production, as an additional control, ICG was also conjugated to the AuNR sidewalls of the AuNR@TiO_2 nanoparticles (denoted as ICG-AuNR@TiO_2) (Figure 3a). To prevent ICG from nonspecifically absorbing to the TiO_2 caps, the porous metal oxide was first reacted with dopamine followed by an excess of NHS–mPEG (MW 20 000). Next, the PEG-conjugated AuNR@ TiO_2 was reacted with cysteamine overnight followed by reacting with NHS–DBCO for 5 h (all of the AuNR@TiO_2 samples used in the following study are PEGylated). The products were then purified by centrifugation and next reacted with azide-ICG using a 1:10 000 molar ratio of AuNR@TiO_2/ICG for 12 h. Using these methods, we were able to obtain ICG-AuNR@TiO_2 samples that showed ~7746 ± 421 ICG conjugated to the sides of the AuNRs, which was close to the number of ICG conjugated to the TiO_2 caps (~6583 ± 567). To test $^1O_2$ generation from ICG conjugated to the tips or sides of AuNR@TiO_2, the dye ABDA was used. Upon $^1O_2$ generation, the fluorescence of the ABDA dye becomes quenched and this decrease can be measured and plotted as a function of irradiation time with 808 nm light. As shown in Figure 3, under 808 nm excitation (power density: 60 mW cm^{-2}), AuNR@TiO_2-ICG nanostructures showed ~2.9-, 2.1-, and 1.8-fold higher $^1O_2$ production as compared with that of the ICG alone, a mixture of ICG and AuNR@TiO_2, and ICG-AuNR@TiO_2, respectively. Considering the higher number of photosensitizers attached to the gold sides of the AuNR@TiO_2 as opposed to the TiO_2 caps, significantly more $^1O_2$ (9.9 ± 0.6% versus 17.5 ± 0.6% decrease in photoluminescence intensity within 25 min irradiation) was produced from the AuNR–TiO_2 nanoparticles that had ICG attached specifically to the TiO_2 caps. It should be pointed out that the $^1O_2$ amounts shown also depend on the distance between the photosensitizer and Au. If assuming the distribution of ICG through the porous TiO_2 cap is even, the average distance between an attached ICG molecule and the AuNR surface is ~21 nm (Figure 2b). At short distances between the metal and ICG, Au will quench the $^1O_2$ emission; at intermediate distances, there will be an enhancement of the $^1O_2$ production because of the surface plasmon effect, while the enhancement factor will fall at longer distances and level off at last.[23] In comparison to AuNR@TiO_2-ICG, a decrease in ABDA fluorescence of ~6.0 ± 1.8, 8.2 ± 1.5, and 9.9 ± 0.6% was seen from ICG alone, a mix of ICG and AuNR@TiO_2, and ICG-

AuNR@TiO_2 samples (ICG conjugated to the AuNR sides). The increase in $^1O_2$ production specifically from the AuNR@TiO_2-ICG nanostructures can be attributed to the stronger localized electric fields that exist at the AuNR tips upon 808 nm excitation.[23,29,30]

The photothermal effect of the AuNR@TiO_2 nanoparticles upon 808 nm laser irradiation (laser power: 3.18 W cm^{-2}) was determined next. As shown in Figure 3b, within 6 min irradiation, the temperature of the AuNR@TiO_2 or AuNR solution showed an increase of ~10 °C, whereas water alone showed only ~2 °C increase in temperature. However, as the AuNR concentrations during these measurements were only ~6.7 nM, it is anticipated that in the body, the local concentrations of AuNR@TiO_2 can be increased by using targeting ligands. At last, in the body, an increase of ~10 °C would lead to a final temperature of ~47 °C, which is sufficient for cell apoptosis and possibly necrosis.[30]

To increase the multimodality of the AuNR@TiO_2 nanostructures, DNA oligonucleotides were next attached to the AuNR sidewalls of AuNR@TiO_2. This was done as dsDNA has shown a natural capacity to associate with some anticancer drugs such as DOX. Upon a local change in temperature, the DNA strands would dehybridize and release any drug loaded.[25,31,32] To study this, after attaching ICG to the TiO_2 tips of AuNR@TiO_2, DNA strands were conjugated specifically to the AuNR surfaces using DNA designs developed earlier by Farokhzad and Chan, where AuNR@ TiO_2-ICG was first conjugated with thiolated 25 mer DNA oligonucleotide followed by hybridizing with a 58 base linker DNA (Figure 1).[31,32] Next, these were further hybridized with short complementary DNA1 in buffer at 37 °C for 1 h, followed by hybridizing with DNA2 and finally DNA3 (Figure 1). To load DOX into the DNA strands, DOX was first dissolved in DMSO and mixed with the DNA-modified AuNR@TiO_2-ICG using a molar ratio of 1:10 000 AuNR@ TiO_2/DOX. After 8 h incubation at room temperature, DOX-loaded AuNR@TiO_2-ICG (DOX-AuNR@TiO_2-ICG) was purified by centrifugation and washed with PBS. To calculate the amount of DOX loaded per AuNR@TiO_2-ICG, the nanocomposites were heated to 65 °C for 30 min. The released DOX was then determined by UV–vis spectroscopy and showed that ~2278 ± 528 DOX could be loaded onto a single AuNR@TiO_2-ICG nanostructure (Figures S5 and S6).

The rate of DOX release from DOX-AuNR@TiO_2-ICG was determined as a function of temperature or NIR light irradiation. For this, DOX was first mixed with dsDNA-functionalized AuNR@TiO_2-ICG in 50% DMSO solution for 8 h at room temperature. Any unbound DOX was next removed by microcentrifuging at 4 °C. To measure DOX release over time, the DOX-AuNR@TiO_2-ICG nanoparticles were dispersed in buffer at 37 °C, and at varying time points ranging from 0 to 25 min, the particles were collected by bulk centrifugation and fluorescence measurements were carried out for the supernatants. As shown in Figure 4, ~2.0% of the initially entrapped DOX was released initially, which could be ascribed to any DOX bound nonspecifically to the PEG-modified TiO_2.[31] After 25 min of incubation at 37 °C, this value increased slightly to ~6.8% of DOX release. For comparison, we tested the release profile after 25 min of incubation at 47 °C, and at this elevated temperature, a very minor increase to ~7.8% of DOX release was observed, which may be due to partial dehybridization of the DNA duplex.[31] Impressively, about ~77.9% of DOX was released after 25 min of photoirradiating with the 808 nm laser (3.18 W cm^{-2}), which was mainly due to the local high temperatures induced near the surface of the AuNRs upon

absorbing NIR light (Figure 4).[33] The photothermal-induced release profile shown by DOX-AuNR@TiO_2-ICG is similar to previous reports using DNA-conjugated AuNRs as drug carriers.[31,34]

Next, to study DOX-AuNR@TiO_2-ICG as potential theranostic agents, we first studied the relative cell cytotoxicity of the ICG-conjugated AuNR@TiO_2 against breast cancer MDA-MB-468 cells. For this, XTT cell viability assays were carried out by incubating ICG, AuNR@TiO_2, AuNR@TiO_2-ICG, and ICG-AuNR@TiO_2 (ICG attached to AuNR tip and side, respectively) with MDA-MB-468 cancer cells for 5 h, where the free and conjugated ICG concentrations were 7.5 μM (Figure S7). As shown in Figure 5a, ICG alone, AuNR@TiO_2, AuNR@TiO_2-ICG, and ICG-AuNR@TiO_2 showed low cell toxicity, demonstrating good biocompatibility.[9] To test the effect of DOX on MDA-MB-468 cells, we next loaded DOX into the DNA-conjugated AuNR@TiO_2-ICG nanostructures and measured cell viability as a function of DOX concentration (Figure 5b).

To test the efficacy of the DOX-AuNR@TiO_2-ICG nanostructures under 808 nm photoirradiation, the DOX-AuNR@TiO_2-ICG nanostructures were next incubated with MDA-MB-468 cells for 5 h. After removing free particles, the cells were photoirradiated with 808 nm light (3.18 W cm^{-2}) for 15 min, followed by incubation for an additional 12 h at 37 °C in the dark. As shown in Figure 6, the DOX-AuNR@TiO_2-ICG nanostructures showed the largest amount of cell death after 808 nm photoirradiation for 15 min with ~74.6% loss in cell viability. In comparison, cells incubated either with free ICG, a mix of AuNR@TiO_2 and ICG, ICG-AuNR@TiO_2, or AuNR@TiO_2-ICG or at equivalent photosensitizer loading showed ~37.2, 42.4, 45.7, and 53.4% decrease in cell viability upon photoirradiation with 808 nm light. The slightly higher cell death of the AuNR@TiO_2-ICG cultured sample was due to the increase in $^1O_2$ produced as compared to the ICG-AuNR@TiO_2 clusters. When cells were incubated with DOX-AuNR@TiO_2 only (no ICG) and photoirradiated, we observed a ~33.0% decrease in cell viability, which was equivalent to that obtained after incubating cells with free DOX (~24.6% decrease in cell viability). However, when DOX-AuNR@TiO_2 was incubated with cells but not photoirradiated, little amount of cells died, indicating much lower amounts of DOX was released in the absence of 808 nm light. To determine how photothermal effects alone affect cell viability, AuNR@TiO_2 nanostructures alone (no DOX, no ICG) were also incubated with cells and photoirradiated. As shown in Figure 6, increases in local temperature led to ~26.9% loss in cell viability. Compared with photothermal therapy PTT or PDT alone, combining PDT and PTT led to an overall increase in cell death.

CONCLUSIONS

In summary, we have successfully designed and validated a novel plasmon-enhanced PDT- and PTT-controlled drug release system for cancer cell therapy. The overall platform consisted of a DNA-conjugated AuNR@TiO_2 nanostructure, where the NIR photosensitizer ICG was conjugated site-specifically to the TiO_2 caps at the tips of the AuNRs and DOX was loaded within DNA strands conjugated to the AuNR sidewalls. Because of the overlap between the surface plasmon resonance peak of AuNR@TiO_2 and the absorbance profile of ICG, placing the photosensitizer at sites where electric field gains were highest upon NIR

excitation led to overall gains in $^1O_2$ production. This increase in PDT coupled with NIR-induced DOX release due to photothermal effects caused higher rates of cell killing against MDA-MB-468 cells through the synergistic effect of PTT, PDT, and chemotherapy.

Supplementary Material

Refer to Web version on PubMed Central for supplementary material.

ACKNOWLEDGMENTS

The research was primarily supported by the National Institute of Health (1R21EB020911–01), NIH (DP2EB020401), Army Research Office under Award # W911NF-14-1-0211, and the National Science Foundation Award # DMR 1420736.

REFERENCES

(1). Wang S; Riedinger A; Li H; Fu C; Liu H; Li L; Liu T; Tan L; Barthel MJ; Pugliese G; De Donato F; Scotto D'Abbusco M; Meng X; Manna L; Meng H; Pellegrino T Plasmonic Copper Sulfide Nanocrystals Exhibiting Near-Infrared Photothermal and Photodynamic Therapeutic Effects. ACS Nano 2015, 9, 1788–1800. [PubMed: 25603353]

(2). Li Y; Wen T; Zhao R; Liu X; Ji T; Wang H; Shi X; Shi J; Wei J; Zhao Y; Wu X; Nie G Localized Electric Field of Plasmonic Nanoplatform Enhanced Photodynamic Tumor Therapy. ACS Nano 2014, 8, 11529–11542. [PubMed: 25375193]

(3). Lucky SS; Idris NM; Li Z; Huang K; Soo KC; Zhang Y Titania Coated Upconversion Nanoparticles for Near-Infrared Light Triggered Photodynamic Therapy. ACS Nano 2015, 9, 191–205. [PubMed: 25564723]

(4). Wang C; Tao H; Cheng L; Liu Z Near-infrared light induced in vivo photodynamic therapy of cancer based on upconversion nanoparticles. Biomaterials 2011, 32, 6145–6154. [PubMed: 21616529]

(5). Liu Y; Liu Y; Bu W; Cheng C; Zuo C; Xiao Q; Sun Y; Ni D; Zhang C; Liu J; Shi J Hypoxia Induced by Upconversion-Based Photodynamic Therapy: Towards Highly Effective Synergistic Bioreductive Therapy in Tumors. Angew. Chem., Int. Ed 2015, 54, 8105–8109.

(6). Lu S; Tu D; Hu P; Xu J; Li R; Wang M; Chen Z; Huang M; Chen X Multifunctional Nano-Bioprobes Based on Rattle-Structured Upconverting Luminescent Nanoparticles. Angew. Chem., Int. Ed 2015, 54, 7915–7919.

(7). Idris NM; Gnanasammandhan MK; Zhang J; Ho PC; Mahendran R; Zhang Y In vivo photodynamic therapy using upconversion nanoparticles as remote-controlled nanotransducers. Nat. Med 2012, 18, 1580–1585. [PubMed: 22983397]

(8). Luo S; Zhang E; Su Y; Cheng T; Shi C A review of NIR dyes in cancer targeting and imaging. Biomaterials 2011, 32, 7127–7138. [PubMed: 21724249]

(9). He L; Brasino M; Mao C; Cho S; Park W; Goodwin AP; Cha JN DNA-Assembled Core-Satellite Upconverting-Metal-Organic Framework Nanoparticle Superstructures for Efficient Photodynamic Therapy. Small 2017, 13, 1700504.

(10). Lismont M; Dreesen L; Wuttke S Metal-Organic Framework Nanoparticles in Photodynamic Therapy: Current Status and Perspectives. Adv. Funct. Mater 2017, 27, 1606314.

(11). Huang P; Lin J; Wang X; Wang Z; Zhang C; He M; Wang K; Chen F; Li Z; Shen G; Cui D; Chen X Light-Triggered Theranostics Based on Photosensitizer-Conjugated Carbon Dots for Simultaneous Enhanced-Fluorescence Imaging and Photodynamic Therapy. Adv. Mater 2012, 24, 5104–5110. [PubMed: 22718562]

(12). Wang S; Huang P; Nie L; Xing R; Liu D; Wang Z; Lin J; Chen S; Niu G; Lu G; Chen X Single Continuous Wave Laser Induced Photodynamic/Plasmonic Photothermal Therapy Using Photosensitizer-Functionalized Gold Nanostars. Adv. Mater 2013, 25, 3055–3061. [PubMed: 23404693]

(13). He L; Liu Y; Liu J; Xiong Y; Zheng J; Liu Y; Tang Z Core-Shell Noble-Metal@Metal-Organic-Framework Nanoparticles with Highly Selective Sensing Property. Angew. Chem., Int. Ed 2013, 52, 3741–3745.

(14). Wadell C; Syrenova S; Langhammer C Plasmonic Hydrogen Sensing with Nanostructured Metal Hydrides. ACS Nano 2014, 8, 11925–11940. [PubMed: 25427244]

(15). Kinkhabwala A; Yu Z; Fan S; Avlasevich Y; Müllen K; Moerner WE Large single-molecule fluorescence enhancements produced by a bowtie nanoantenna. Nat. Photon 2009, 3, 654–657.

(16). Murdoch M; Waterhouse GIN; Nadeem MA; Metson JB; Keane MA; Howe RF; Llorca J; Idriss H The effect of gold loading and particle size on photocatalytic hydrogen production from ethanol over Au/TiO2 nanoparticles. Nat. Chem 2011, 3, 489–492. [PubMed: 21602866]

(17). Linic S; Aslam U; Boerigter C; Morabito M Photochemical transformations on plasmonic metal nanoparticles. Nat. Mater 2015, 14, 567–576. [PubMed: 25990912]

(18). Kale MJ; Avanesian T; Christopher P Direct Photocatalysis by Plasmonic Nanostructures. ACS Catal 2014, 4, 116–128.

(19). Liu L; Ouyang S; Ye J Gold-Nanorod-Photosensitized Titanium Dioxide with Wide-Range Visible-Light Harvesting Based on Localized Surface Plasmon Resonance. Angew. Chem., Int. Ed 2013, 52, 6689–6693.

(20). Yuan H; Fales AM; Vo-Dinh T TAT Peptide-Functionalized Gold Nanostars: Enhanced Intracellular Delivery and Efficient NIR Photothermal Therapy Using Ultralow Irradiance. J. Am. Chem. Soc 2012, 134, 11358–11361. [PubMed: 22734608]

(21). He L; Dragavon J; Cho S; Mao C; Yildirim A; Ma K; Chattaraj R; Goodwin AP; Park W; Cha JN Self-assembled gold nanostar-NaYF4:Yb/Er clusters for multimodal imaging, photothermal and photodynamic therapy. J. Mater. Chem. B 2016, 4, 4455–4461.

(22). Greybush NJ; Saboktakin M; Ye X; Giovampaola CD; Oh SJ; Berry NE; Engheta N; Murray CB; Kagan CR Plasmon-Enhanced Upconversion Luminescence in Single Nanophosphor-Nanorod Heterodimers Formed through Template-Assisted Self-Assembly. ACS Nano 2014, 8, 9482–9491. [PubMed: 25182662]

(23). Planas O; Macia N; Agut M; Nonell S; Heyne B Distance-Dependent Plasmon-Enhanced Singlet Oxygen Production and Emission for Bacterial Inactivation. J. Am. Chem. Soc 2016, 138, 2762–2768. [PubMed: 26867005]

(24). Fales AM; Yuan H; Vo-Dinh T Silica-Coated Gold Nanostars for Combined Surface-Enhanced Raman Scattering (SERS) Detection and Singlet-Oxygen Generation: A Potential Nanoplatform for Theranostics. Langmuir 2011, 27, 12186–12190. [PubMed: 21859159]

(25). Mohan P; Rapoport N Doxorubicin as a Molecular Nanotheranostic Agent: Effect of Doxorubicin Encapsulation in Micelles or Nanoemulsions on the Ultrasound-Mediated Intracellular Delivery and Nuclear Trafficking. Mol. Pharmaceutics 2010, 7, 1959–1973.

(26). Ye X; Zheng C; Chen J; Gao Y; Murray CB Using Binary Surfactant Mixtures To Simultaneously Improve the Dimensional Tunability and Monodispersity in the Seeded Growth of Gold Nanorods. Nano Lett 2013, 13, 765–771. [PubMed: 23286198]

(27). Wu B; Liu D; Mubeen S; Chuong TT; Moskovits M; Stucky GD Anisotropic Growth of TiO2 onto Gold Nanorods for Plasmon-Enhanced Hydrogen Production from Water Reduction. J. Am. Chem. Soc 2016, 138, 1114–1117. [PubMed: 26807600]

(28). Urdaneta I; Keller A; Atabek O; Palma JL; Finkelstein-Shapiro D; Tarakeshwar P; Mujica V; Calatayud M Dopamine Adsorption on TiO2 Anatase Surfaces. J. Phys. Chem. C 2014, 118, 20688–20693.

(29). Liu N; Tang ML; Hentschel M; Giessen H; Alivisatos AP Nanoantenna-enhanced gas sensing in a single tailored nanofocus. Nat. Mater 2011, 10, 631–636. [PubMed: 21572410]

(30). He L; Mao C; Cho S; Ma K; Xi W; Bowman CN; Park W; Cha JN Experimental and theoretical photoluminescence studies in nucleic acid assembled gold-upconverting nanoparticle clusters. Nanoscale 2015, 7, 17254–17260. [PubMed: 26427014]

(31). Raeesi V; Chou LYT; Chan WCW Tuning the Drug Loading and Release of DNA-Assembled Gold-Nanorod Super-structures. Adv. Mater 2016, 28, 8511–8518. [PubMed: 27501857]

(32). Xiao Z; Ji C; Shi J; Pridgen EM; Frieder J; Wu J; Farokhzad OC DNA Self-Assembly of Targeted Near-Infrared-Responsive Gold Nanoparticles for Cancer Thermo-Chemotherapy. Angew. Chem., Int. Ed 2012, 51, 11853–11857.

(33). Baffou G; Girard C; Quidant R Mapping Heat Origin in Plasmonic Structures. Phys. Rev. Lett 2010, 104, 136805. [PubMed: 20481904]

(34). Wang D; Xu Z; Yu H; Chen X; Feng B; Cui Z; Lin B; Yin Q; Zhang Z; Chen C; Wang J; Zhang W; Li Y Treatment of metastatic breast cancer by combination of chemotherapy and photothermal ablation using doxorubicin-loaded DNA wrapped gold nanorods. Biomaterials 2014, 35, 8374–8384. [PubMed: 24996756]

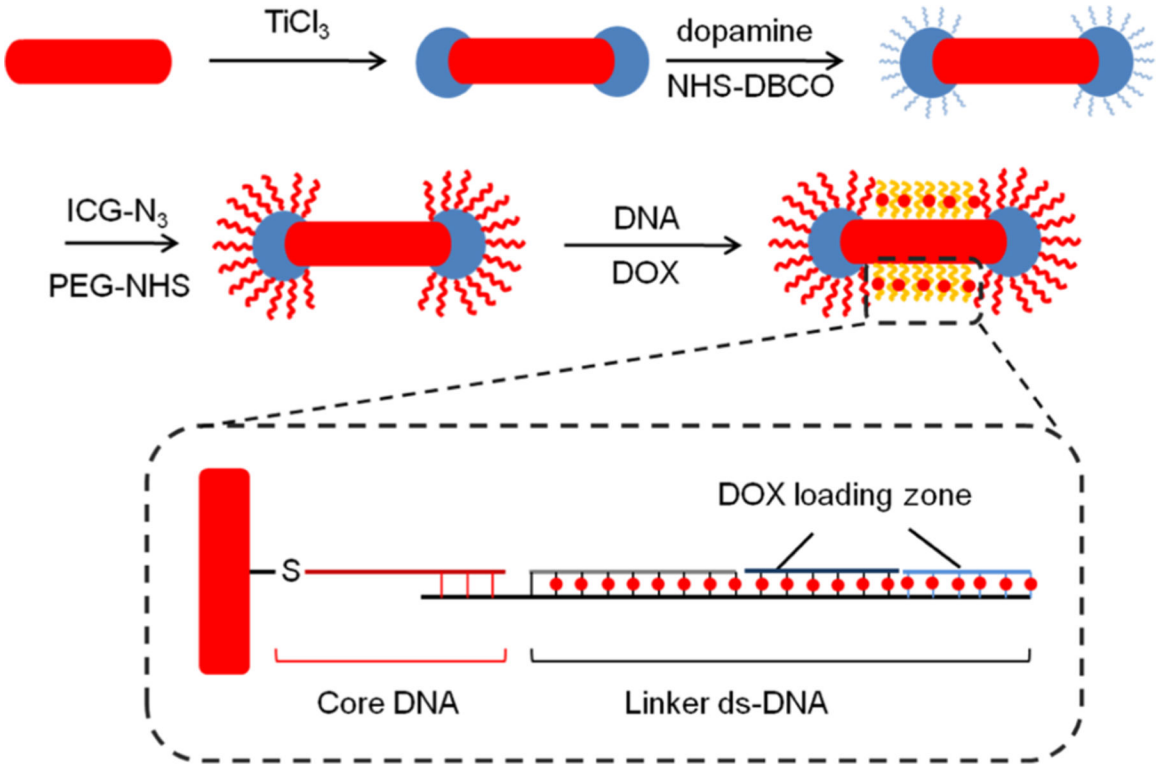

Figure 1.

Schematic showing the overall process to produce ICG and DOX-loaded TiO_2-modified AuNRs. First, porous TiO_2 caps were synthesized at the tips of AuNRs (AuNR@TiO_2). Next, ICG was site-specifically attached to TiO_2 by first reacting with dopamine followed by NHS–DBCO and azide-functionalized ICG. The ICG-conjugated AuNR@TiO_2 was next reacted with thiolated-CG-containing DNA strands that were then loaded with DOX.

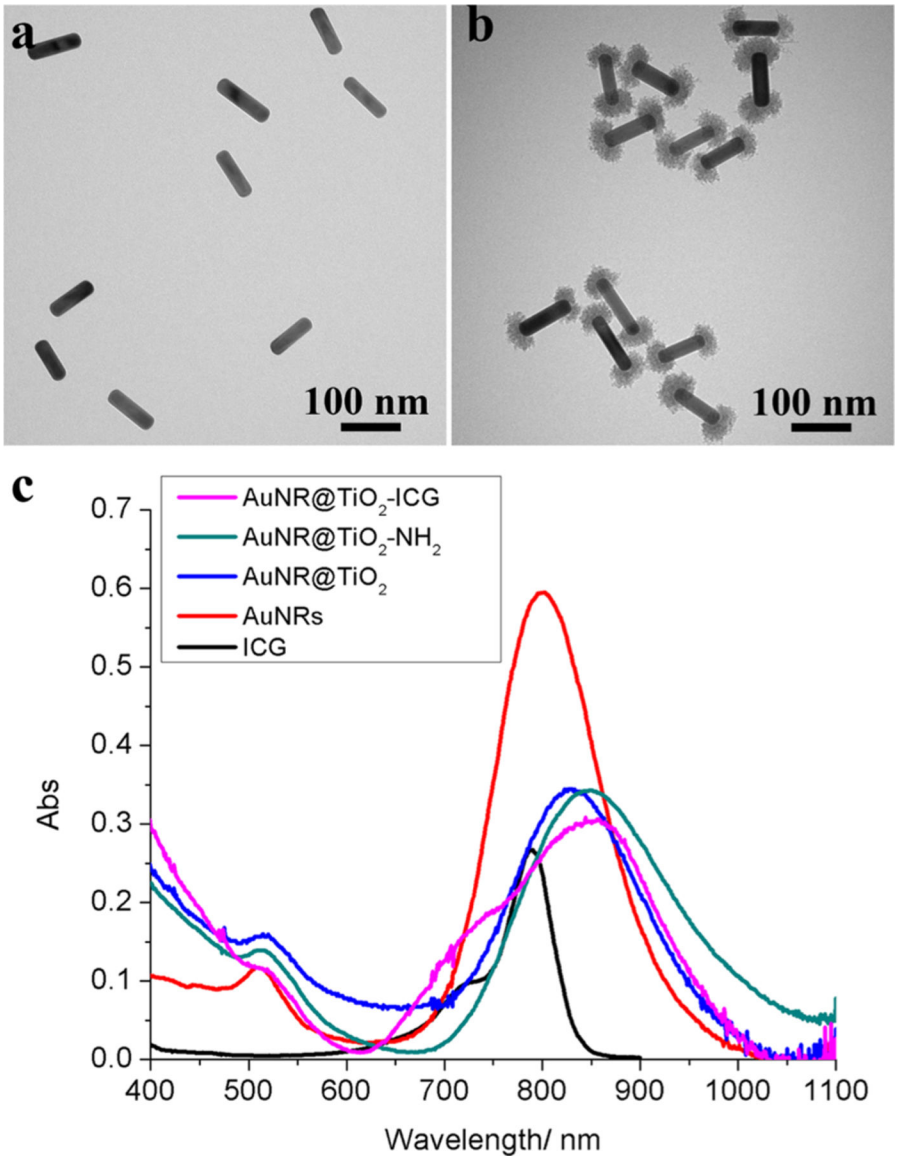

Figure 2.

Transmission electron microscopy images of (a) AuNRs and (b) AuNRs after growing ~21 nm caps of TiO_2 at the tips. (c) UV–vis absorbance spectra of free ICG, AuNRs, AuNR@TiO_2 before and after dopamine modification, and AuNR@TiO_2-ICG.

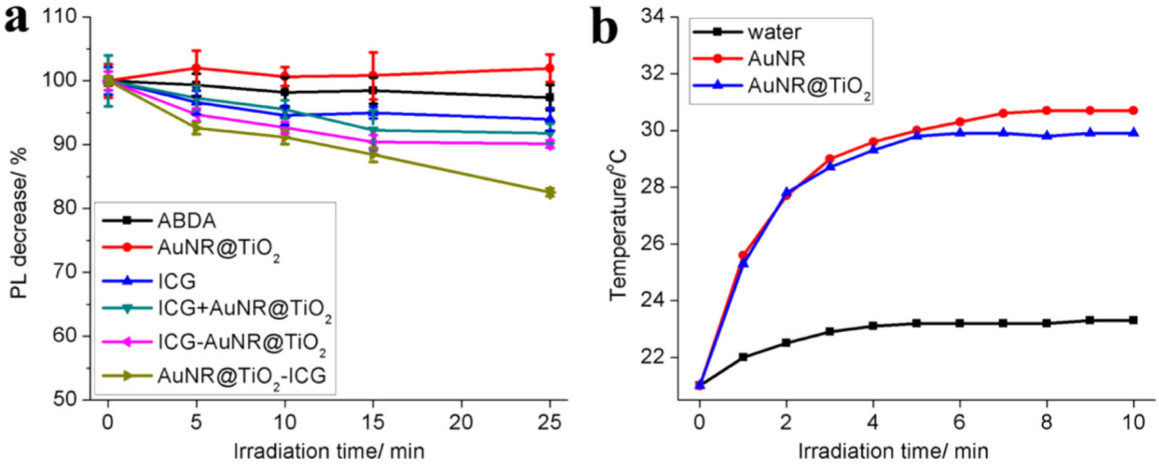

Figure 3.

(a) Singlet oxygen generated from ICG, mixtures of ICG and AuNR@TiO_2, ICG-AuNR@TiO_2, and AuNR@TiO_2-ICG under 808 nm light irradiation (ICG/ABDA = 1:1) (60 mW cm^{-2}) and (b) photothermal effect of AuNRs and AuNR@TiO_2 under 808 nm laser irradiation (100 μL 6.7 nM AuNRs solution) (laser power: 3.18 W cm^{-2}).

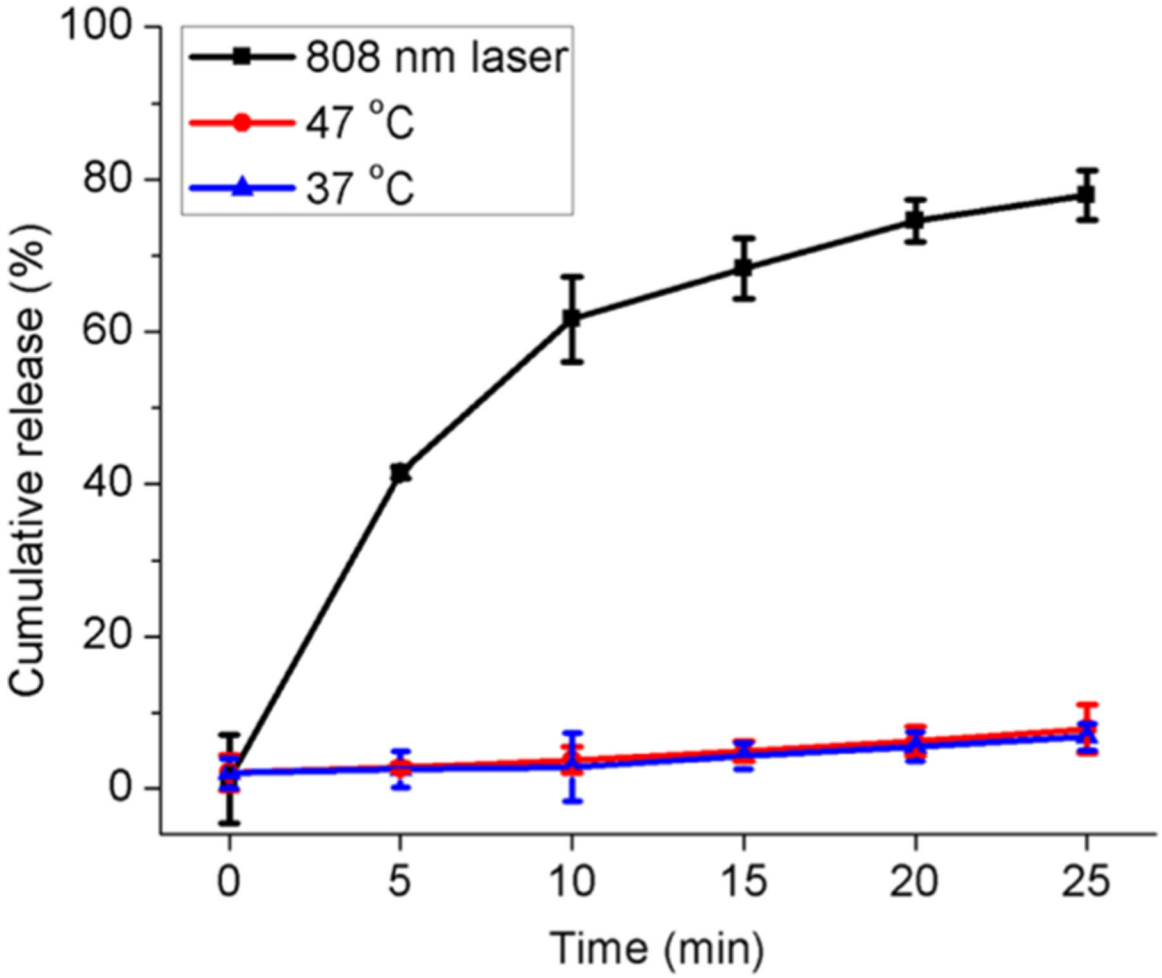

Figure 4.
Cumulative DOX release profiles from DOX-AuNR@TiO_2-ICG nanocomposites at different temperatures and NIR laser excitation.

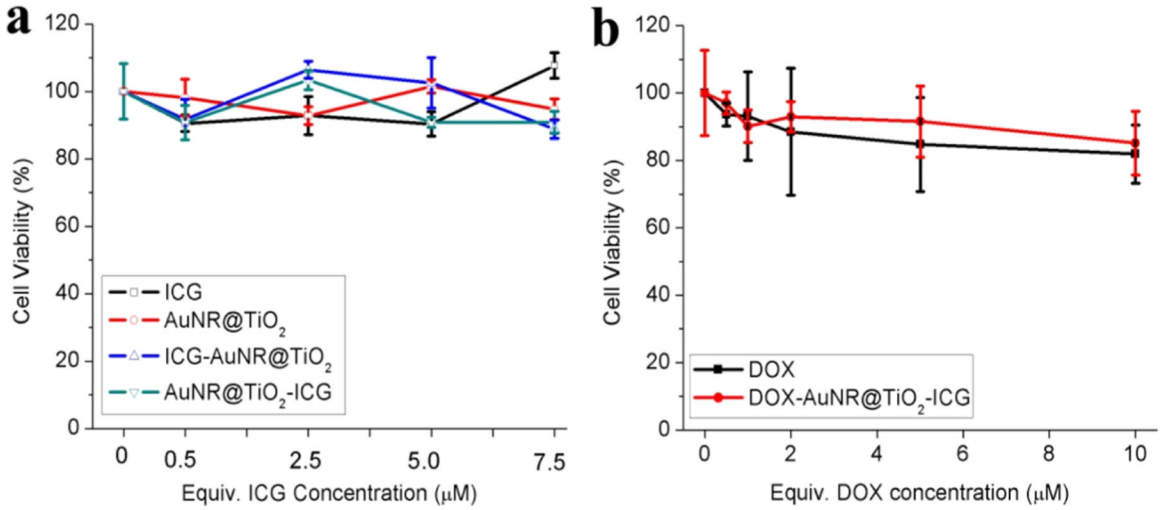

Figure 5.

In vitro cell viability assay of MDA-MB-468 cells incubated with (a) ICG, AuNR@TiO_2, ICG-AuNR@TiO_2, and AuNR@TiO_2-ICG in the dark for 5 h and (b) DOX and DOX-AuNR@TiO_2 in the dark for 5 h.

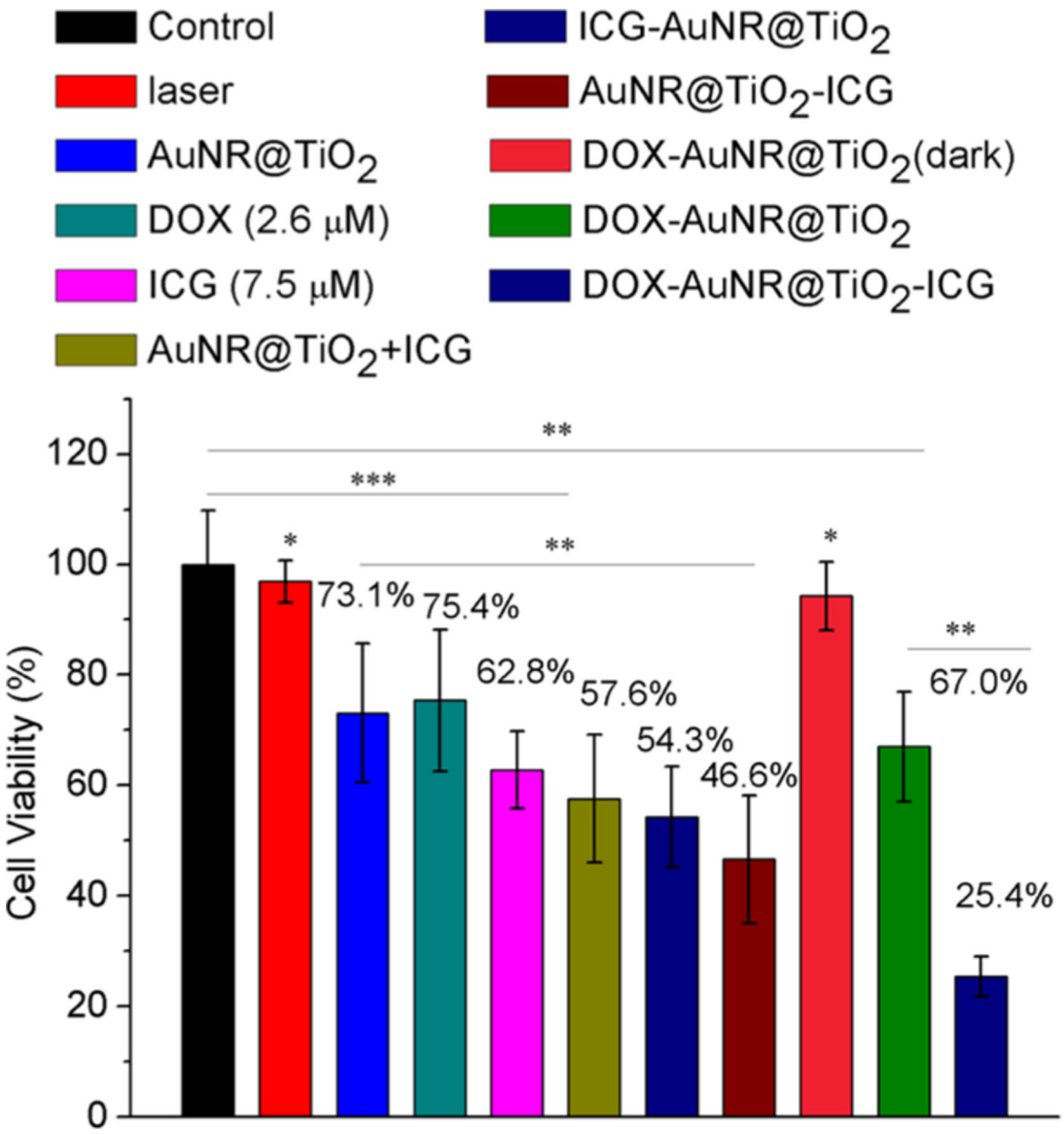

Figure 6.

Quantitative analysis of MDA-MB-468 cell viabilities with ICG, DOX, AuNR@TiO_2, mixtures of ICG and AuNR@TiO_2, ICG-AuNR@TiO_2, and AuNR@TiO_2-ICG with and without DOX. All samples were irradiated with an 808 nm laser light for 15 min. *$p < 0.05$, **$p < 10^{-2}$ ***$p < 10^{-4}$ relative to control (black).